Evidence of middle Holocene landslide-generated tsunamis recorded in lake sediments from Saqqaq, West Greenland

Niels J. Korsgaard[1], Kristian Svennevig[1], Anne S. Søndergaard[2], Gregor Luetzenburg[1,3], Mimmi Oksman[1], and Nicolaj K. Larsen[4]

[1] Department of Glaciology and Climate, Geological Survey of Denmark and Greenland, Copenhagen, Denmark
[2] Laboratory of Ion Beam Physics, ETH Zürich, Switzerland
[3] Department of Geosciences and Natural Resource Management, University of Copenhagen, Copenhagen, Denmark
[4] Globe Institute, University of Copenhagen, Copenhagen, Denmark

Correspondence to: Niels J. Korsgaard (njk@geus.dk)

Abstract.

The Vaigat strait (*Sullorsuaq*) in West Greenland is well known for its susceptibility to landslides and historical landslide-generated tsunamis. Recent mapping of the seabed in the Vaigat strait has revealed several prehistoric giga-scale (volumes of 10^9 m^3), tsunamigenic landslides. However, the timing of these giga-scale tsunamis is largely unconstrained, but they are assumed to have occurred after the last deglaciation. Here, we report on lake sediment core records from four coastal lakes located between 19 and 91 m above sea level (a.s.l.) on the Saqqaq foreland at the eastern end of Vaigat strait. We use a multiproxy approach including X-ray fluorescence (XRF), and magnetic susceptibility core scanning along with a screening for marine diatoms to identify at least two tsunami deposits in two of the four sediment cores. Radiocarbon dating of aquatic macrofossils and bulk samples suggest that the tsunami events occurred at c. 7.6 and 7.3 cal. ka BP. Using a previously published relative sea level curve from Vaskebugt, Arveprinsen Ejland (*Alluttoq*), located 40 km southeast of Saqqaq, we infer wave run-up heights of c. 41-66 and 45-70 m, respectively for the two tsunami events. These run-up heights from prehistoric tsunamis are one-to-two orders of magnitude higher than the historic landslide-tsunami run-up heights at Saqqaq which only reached an elevation of c. 3 m in November 2000. While we found deposits from two tsunami events in the lake sediments, landforms from at least nine giga-scale landslides are present on the seafloor of Vaigat. We infer that these deposits probably represent the two most recent tsunamis identified in Vaigat strait and the older tsunamis must have happened between the last deglaciation and the oldest sediment in the lakes i.e., between c. 10.0 and 8.5 cal. ka BP.

1 Introduction

Landslide-tsunamis are among the most devastating natural disasters in fjord settings with several recent examples from Norway, Alaska, and Chile (e.g., Blikra et al., 2006; Sepulveda et al., 2010; Higman et al., 2018; Svennevig et al., 2020, 2023a). A landslide-tsunami occurs when large rock masses suddenly fail and slide into a water body, usually in the form of a

rock avalanche (*sensu* Hungr et al., 2014 and Hermanns et al., 2021), displacing large amounts of water that travel through the fjord rising to a tsunami wave that can inundate nearby coastal areas (Hermanns et al, 2013). As such, landslides with tsunamigenic potential pose a direct threat to coastal communities, and under a warming climate they are expected to occur more frequently (Patton et al., 2019).

The Vaigat strait (*Sullorsuaq*; Fig. 1) in West Greenland has experienced two landslide-triggered tsunamis in 1952 and 2000 (Pedersen et al., 2002; Dahl-Jensen et al., 2004; Svennevig et al., 2023a). In 1952, the tsunami caused damage to infrastructure in the settlement of Qullissat and a loss of one human life (Svennevig et al., 2023a). In 2000, the landslide at Paatuut generated large waves which hit the settlement of Saqqaq, while the now abandoned settlement of Qullissat, experienced severe damage to buildings at lower elevations (Pedersen et al., 2002). In 2021, a third landslide occurred at Assapaat in between the Niiortuut and the Paatuut landslide (Fig. 1). Although c. 4×10^6 m^3 (0.004 km^3) of material entered the Vaigat strait, no tsunami was observed, which is probably due to local topographical control and the specific dynamics of this landslide (Svennevig et al., 2022). It has recently been showed that the historical landslides in Vaigat strait were preconditioned by permafrost degradation (Svennevig et al., 2022, 2023a). Farther north at Karrat Isfjord, a large rock avalanche triggered a tsunami in June 2017 that inundated the nearby settlement of Nuugaatsiaq and cost four human lives (Paris et al., 2019; Svennevig et al., 2020) showing that landslides are also occurring outside of the Vaigat strait. Svennevig et al. (2020) mapped three areas of continued slope deformation near the 2017 landslide and today the two settlements of Illorsuit and Nuugaatsiaq with a combined 170 inhabitants are closed due to continued risk of landslide induced tsunamis in the area.

Svennevig (2019) compiled a preliminary inventory of landslides in Greenland based on available Digital Elevation Models (DEMs) and bathymetric data. In the Vaigat strait, nine large underwater landslide deposits were mapped. They are recognizable by their hummocky and blocky topography in the otherwise smooth U-shaped glacial trough with a Holocene sediment cover comprising the bottom the Vaigat strait (Fig. 1.) (Svennevig et al., 2023b). Seismic profiles from Vaigat strait show the presence of localized chaotic accumulations of sediment interpreted as either old submarine slides or submarine aggradations from subaerial landslides, with a general thickness of 50-100 m that can locally exceed 200 m (Marcussen et al., 2001; Pedersen et al., 2002). Based on the long runout, large volumes, and giant displaced blocks Svennevig et al. (2023b) suggests that these rock avalanches had a significant tsunamigenic potential, which should leave onshore evidence of tsunamis. However, nothing is known of when the landslides occurred after the last deglaciation or what magnitude the tsunamis could have generated.

Coastal lake sediments are excellent archives for capturing and preserving evidence of past tsunami events as these events have a distinct lithological signature that is different than the normal lacustrine sedimentation (e.g., Bondevik et al., 1997a; Long et al., 2015). If several lakes are cored in the same area at different elevations i.e., staircase approach the sedimentological records can furthermore be used to estimate the run-up height of a tsunami and thus its magnitude (e.g., Bondevik et al., 1997b).

Evidence of tsunamis is in general rare in Greenland and has only been encountered by coincidence three times in relation to paleoclimatic studies or relative sea level (RSL) reconstructions using lake sediment records. In Loon Lake in East Greenland and in the Ammassalik area in Southeast Greenland deposits attributed to the Storegga submarine slide have been described (Wagner et al. 2006; Long et al., 2008). In Disko Bugt (*Qeqertarsuup Tunua)* in West Greenland, tsunami deposits attributed to rolling icebergs were identified (Long et al., 2015).

Until now no systematic study of lake sediment cores has been undertaken to reconstruct the Holocene tsunami history in Vaigat strait. In this study we use six lake sediment cores from the coastal foreland at Saqqaq in the Vaigat strait to constrain the timing and magnitude of prehistoric tsunamis.

2 Study site: Saqqaq foreland and surroundings

The settlement of Saqqaq (population 132 in 2020) in West Greenland is situated on the southern coast of the Saqqaq foreland protruding into Vaigat (Fig. 1). The Vaigat strait is generally between 500 and 600 m deep with depths of up to 620 m south of Saqqaq, except where landslide deposits and dykes and sills (Paleocene intrusions) are present. The elevation of the foreland gradually increases from sea level up to c. 200 m about 5 km from the coast at the foot of the c. 900 m high mountains (Fig. 2). West of the foreland lies Saqqaqdalen which is a valley with a flat floor consisting of a fluvial plain that continues into the Umîvik delta.

This exposed coastal configuration and the multiple lakes situated at different elevations, also known as a staircase, makes the Saqqaq foreland ideal for retaining evidence of past tsunamis to determine the timing and elevation of tsunami run-up. Weidick & Bennike (2007) provides a minimum age of the last deglaciation around 10 cal. ka BP from dating marine shells at 70 m a.s.l. (Fig. 2). Susceptibility of the lakes to inundation from tsunami waves would have been higher in the Early Holocene considering Saqqaqdalen would have been submerged more than 70 m due to glacial isostatic subsidence, and in the middle Holocene the glacial isostatic subsidence would depress the landscape c. 6-25 m (5.8-7.6 cal. ka BP) relative to today.

The landscape surrounding the lakes consists of undulating bedrock surfaces with a thin and discontinuous sediment cover. The bedrock of the Saqqaq foreland generally consists of Precambrian granodioritic augen gneiss (Garde & Steenfelt, 1994). An outcrop of the Kingittoq Member, a Late Cretaceous (Cenomanian) fluvial and deltaic deposit is located on the mountain slopes (Fig. 2), and consists of successions of mudstones, heteroliths and well-sorted sandstones (Pulvertaft, 1989). At the type section of this member 25 km northwest of Saqqaq, sandstone sheets are often overlain by carbonaceous heterolithic mudstones with thin coal beds (Dam et al., 2009). At Saqqaq, the Kingittoq Member is more coarse-grained and consists of cross-bedded pebble conglomerates, with no coal beds reported (Pulvertaft, 1989).

2.1 The November 2000 tsunami in Saqqaq

Detailed observations of run-up heights for the tsunami in Saqqaq in November 2000 have not previously been published. To compare these to the paleotsunamis reported below we have mapped the run-up height of this event using recognizable buildings in photographs taken after the event (Fig. 3A). As the land was snow covered at the time of the event and the tsunami occurred at mean tide, the maximum run-up is readily recognizable. West of the peninsula, the maximum run-up height was c. 3 m whereas east of the peninsula, no visible tsunami run-up was observed (Fig. 3A). Saqqaq is not in direct line of sight to the Paatuut landslide 55 km away (Fig. 1) thus the waves that were observed have been reflected and refracted.

3 Methods

Four lakes were selected using high-resolution satellite images and a 2 m resolution DEM (SDFI, 2018). Lakes with small, local catchments were chosen and lakes with large tributaries or visible influx of sediment were avoided. Their sill elevations range from 19 m to 91 m a.s.l. (Fig. 2). The lake depth was measured using a GARMIN echo sounder and the sediment cores were obtained at the deepest part of the lake by hammering a 60 mm piston corer into the lake floor from a Zodiac inflatable boat.

After recovering the sediment cores, they were kept upright and drained before shipped to Denmark where they were stored under refrigerated conditions at 2-4 °C. In the laboratory, the cores were split, and the stratigraphy described. The cores were scanned using an ITRAX core scanner to obtain X-ray fluorescence (XRF), X-ray imagery, magnetic susceptibility (MS) and an optical line scan image. The cores were scanned with a 1 mm resolution using a standard setting of 30 kV and 50 mA for the X-ray fluorescence scanning and a dwell time of 30 s. The X-ray settings were 3 kV and 50 mA with a dwell time of 1 second and a step size of 0.2 mm. Both XRF and X-ray used a Rh tube. The MS has a step size of 4 mm, and the optical scan has a resolution of 0.047 mm. The ITRAX core scanner provides counts of c. 40 elements, and it has been used to identify tsunami deposits onshore and in lake cores (e.g., Chagué-Goff et al., 2017; Shinozaki, 2021). In this study, we use the element Titanium (Ti) as a proxy for minerogenic input to the lake (i.e.., tsunami deposits) and the element ratio Ca/Fe as a proxy for marine influence in the sediment. Titanium is suitable to differentiate between marine with a high minerogenic content, and lacustrine gyttja deposits with low minerogenic content. As Ti is a common constituent of rocks such as gneisses or schists, it primarily indicates a terrigenous continental source (Rothwell & Croudace, 2015). In our setting, high Ti values are interpreted as minerogenic deposits flushed into the lake from either shoreline or onshore surroundings as the tsunami wave loses energy and the water runs back to the sea. The Ca/Fe ratio is used as a proxy for input of biogenic carbonates of marine origin (Ca) relative to detrital clay (Fe) of terrigenous origin into the lake and can be used to indicate tsunami deposits (Chagué-Goff et al., 2017).

We describe the tsunami deposits in the cores using typical stratigraphic signatures identified by Bondevik et al. (1997a) and summarized by Long et al. (2015). These are stratigraphical signatures in lake sediments that have been found in lakes inundated by the tsunami waves from the Storegga submarine landslide off the coast of Norway. Here, the base of the tsunami deposit consists of massive or graded sand suggesting a rapid deposition from suspension overlying an erosional unconformity. The erosional unconformity was caused by the turbulence from the tsunami wave as it crossed the lake threshold. Above the sand, a facies termed "organic conglomerate" may be present. This facies consists of coarse organic detritus with large rip-up clasts of gyttja, peat, and silt. The large rip-up clasts are of irregular form and sizes and occur with twigs and plant fragments in a matrix of gyttja and silt. Lenses of sand may also be present (Bondevik et al., 1997a). One criteria from Bondevik et al, (1997a) we are not able to test is the lateral extent of the tsunami deposits as we did not survey the lake stratigraphy with multiple cores during field work.

The chronology is based on AMS radiocarbon (^{14}C) dating of aquatic plant macrofossils (mosses) or bulk sediment samples, as we were unable to identify any terrestrial macrofossils. The local bedrock consists of non-calcareous rocks; hence this specific problem can be excluded when using aquatic macrofossils or bulk sediment samples for dating the cores. The macrofossil samples are unspecified aquatic mosses (bryophytes) and this is not without implications for how the obtained ages can be used. Aquatic mosses will fix reservoir-aged dissolved CO2 from the water column or sediment pore water in quantities large enough to introduce old-carbon reservoir effects to the radiocarbon dating of the moss (Marty and Myrbo, 2014). Radiocarbon ages above the tsunami unit also have complications. In principle, the sediment just above the tsunami unit should show the minimum age of the tsunami. However, Bondevik et al. (1997b) found that for lakes in western Norway radiocarbon ages above the tsunami deposits are commonly older than the actual age of the tsunami inundating the lakes.

In total, we dated twelve samples to constrain the age of the cores and provide age control of tsunami events (Table 1). We used three sampling strategies to determine the age of a tsunami deposit. To provide a maximum age of the events we dated samples below the tsunami deposit under an erosional unconformity. Bulk sampling of rip-up clasts or macrofossils embedded in the tsunami deposit were also dated to provide a maximum age, while a minimum age is obtained by dating lacustrine samples above the tsunami deposit where lacustrine sediments re-occurred. The ^{14}C ages were calibrated into calendar years using the OxCal v4.4 (Bronk Ramsey, 2009) and the IntCal20 calibration curve (Reimer et al., 2020).

There is no local RSL curve for Saqqaq, so we recalibrate existing isolation basin radiocarbon dates from Long et al. (1999) from Vaskebugt (Kangerluarsuk), Arveprinsen Ejland (Alluttoq) (see Fig. 6). This location is situated 40 km to the southeast of Saqqaq (Fig. 8) and would have deglaciated a few hundred years later than Saqqaq, which would have seen slightly higher uplift rates (Long et al., 1999). Consequently, when using the Arveprinsen Ejland RSL curve on Saqqaq, it will underestimate how much uplift has occurred at any given time.

In addition to the radiocarbon dates used for the RSL curve from Long et al. (1999) we also use radiocarbon dates from Weidick (1968, 1972) where shells provide a minimum age of the last deglaciation at Saqqaq (Weidick, 1968) and a minimum height of the RSL at that time (Weidick, 1972). We have recalibrated all samples, so they are standardized with the radiocarbon ages used in this study (Table 1). The ^{14}C ages for samples from this study and Long et al. (1999) were calibrated into calendar years using the OxCal v4.4 (Bronk Ramsey, 2009) and the IntCal20 calibration curve (Reimer et al., 2020). K-994 has not been normalised for isotopic fractionation to a delta ^{13}C value of -25 permille i.e., we have added 400 years before calibrating the date into calendar years using Marine20 (Heaton et al., 2020) using a local dR= -49±59 from West Greenland (Pearce et al., 2023).

We screened sediment core SAQ21-06 from relevant depths for diatom assemblages to find marine species that could be used as indicator of marine water intrusion to lakes. In total five diatom microscopy slides were prepared according to Battarbee et al. (2001). We treated c. 0.2-0.5 grams of fresh sediment with 10 % hydrochloric acid (HCl) and 30 % hydrogen peroxide (H2O2) in a water bath for 4 hours to remove carbonates and organic material from the sediment. Samples were rinsed with distilled water and slides were mounted using Naphrax ® with a refractive index of 1.73. Diatoms were identified with an Olympus BX51 light microscope using phase contrast optics at 1000x magnification.

4 Results

We retrived four lake cores of which two contain tsunami deposits and another two help constrain the age of the tsunami deposits. Lake coring site characteristics are summarized in Table 2 and cores are plotted with sediment proxies in Fig. 4 and Fig. 5. All core lengths reflect the thickness of the sediment package until the corer encountered bedrock or an impenetrable substrate. The lakes are situated below the marine limit and marine sediments should be expected in the bottom of the cores. However, in several of our attempts to penetrate the deepest part of the succession the core tubes fractured probably because of the stiff nature of the sediments. Accordingly, we were unable to penetrate the entire succession and retreive marine sediments.

4.1 Lacustrine and glaciolacustrine deposits

4.1.1. Gyttja facies

The organic-rich gyttja is the main lithology in all cores. It is brown to brownish-grey and vary from being finely laminated to massive in composition (Fig. 4, Fig. 5). Both the laminated and massive gyttja have very low minerogenic content characterized by low Ti and MS values.

4.1.3 Interpretation of gyttja facies

The gyttja facies is interpreted as lacustrine sediments deposited under normal conditions in the lakes withput input from glaciers. The variations in gyttja composition between the lake records probably reflect different lake sizes, and depths as well as catchment properties.

195

4.3 Tsunami deposits

We have identified deposits from two tsunami events, T1 and T2, which are both present in cores SAQ21-06 and SAQ21-09 (Fig. 4 and Fig. 5).

200 #### 4.2.1 Tsunami unit 1 (T1)

The younger (T1) tsunami deposit is 28 and 41 cm thick in SAQ21-06 and SAQ21-09, respectively. In both cores, it has a distinct erosional base followed by a layer of massive coarse to very coarse sand (grain size 1-2 mm). In SAQ21-09, T1 has eroded into the sediments of T2, while in SAQ21-06 there is a laminated gyttja facies in between the two tsunami deposits, making it possible to separate the T1 from T2. In SAQ21-09 there is a 3.5 cm massive sand layer above the erosional
205 unconformity. The massive sand is followed by 38 cm of organic conglomerate consisting of irregular clasts composed of silt or sand and with plant fragments. Some of the rip-up clasts consist of laminated gyttja and the size of the clasts decreases upwards in T1 with several lenses of coarse sand visible within the organic conglomerate. The contact to the massive gyttja above is transitional for 1-2 cm .

210 In SAQ21-06 the corresponding massive sand layer is 0.5 cm thick with an erosional unconformity at the base. It is overlain by 27 cm of organic conglomerate consisting of large rip-up clasts of irregular form and size and with plant fragments, silts and sands. There are at least two erosional unconformities inside the organic conglomerate with layers of sand. A thin layer of sand constitutes the sharp contact between the organic conglomerate and 20 cm of lacustrine laminated gyttja above.

215 Our sediment proxies (Fig. 4) MS, Ca/Fe, and Ti are all very high at the massive sand at the base of the tsunami sediments and where sand lenses are located in the organic conglomerates making the sediment proxies much more variable relative to the gyttja.

4.3.1 Tsunami unit (T2)

In core SAQ21-09 the oldest tsunami unit (T2) makes up the bottom of the core. Here, the top of the 26 cm thick T2 sediments has been eroded by the overlying T1. In the other core, SAQ21-06, T2 is 7 cm thick and enclosed by laminated gyttja above and below.

The base of the T2 in core SAQ21-09 consists of a 0.2 cm layer of massive coarse sand and very coarse sand. Most of the coarse sand flushed to the bottom of the tube when it was sealed and had to be cut off the main core. It is not shown here as primary sedimentary structures were not preserved. Above the massive sand is a 3 cm thick layer of organic detritus with sand grading upwards, which is followed by 6 cm of coarse organic detritus with small gyttja clasts and plant fragments in a matrix of fine-medium sand. Above is a 8 cm block of laminated gyttja, where the laminations of the gyttja are cross-cut by the unit below, indicating that the gyttja was deposited prior to the unit below and has been displaced subsequently. Then follows a 0.1 cm layer of coarse sand grading to medium-fine for 1 cm. The contact between the coarse sand and the laminated gyttja below is sharp. Overlying is 8 cm of coarse organic detritus with gyttja clasts and plant fragments and fine to medium sand.

The 7 cm thick T2 unit in SAQ21-06 consist of coarse organic detritus with clasts with a thin layer of sand at its base and a sharp contact without visible erosion of the laminated gyttja below. There are small clasts of gyttja and more plant fragments than in SAQ21-09. T2 has a sharp contact to the laminated gyttja above.

Our sediment proxies (Fig. 4) MS, Ca/Fe, and Ti are all very high in the organic detritus facies and low in the tilted block laminated gyttja in SAQ21-09. In the upper organic detritus facies in SAQ21-09 the variability is greater due to larger clasts.

4.3.1 Interpretation of tsunami facies (T1 and T2)

We interpret T1 and T2 as tsunami deposits as they contain many of the diagnostic characteristics described by Bondevik et al. (1997a). The lowest part of T1 and T2 consists of coarse to very coarse sands with clear erosional unconformities at the base, the sand is angular and similar to the sand found in the terrain surrounding the lake. Thus, it is likely that the massive, coarse sand has been flushed into the lakes from the surroundings when the tsunami wave withdrew. In both deposits, this is followed by an organic conglomerate with rip-up clasts, sands, and plant fragments. The organic-rich conglomerates have erosional unconformities and lenses of sand which we interpret as caused by subsequent waves from the same landslide-tsunami wave train. We interpret the deposits in the two cores as tsunami deposits. While identification of the tsunami deposits is based on visual description of sediments and structures, and sedimentological proxies, the correlation of the units between the two cores with tsunami deposits is primarily based on the laminated gyttja separating the two tsunami units T1 and T2 in core SAQ21-06, constrained by the age control. This correlation is supported by the visual appearance and sedimentological

proxies of T1 and T2 in the two cores. Since we did not survey the entire lake stratigraphy, we cannot exclude the small possibility that the c. 42 cm unit of laminated gyttja could be a large rip-up clast and T1 and T2 may be the result one tsunami event.

The T2 tsunami facies in the two lakes have the same signatures and we correlate them based on visual appearance. Although T2 has the same general appearance in the two lakes, there are some notable differences. These reflect that lake SAQ21-09 is much more exposed to tsunamis and has experienced much more turbulence and erosion when invaded by the tsunami compared to SAQ21-06. SAQ21-09, has a coarser sand fraction at the base and no gyttja below the base of the tsunami facies which is standing directly on top of an impenetrable substrate. The sediment core also has sand lenses from distinct waves from the same landslide-tsunami wave train, indicating that aspect to the strait and exposure to the incoming tsunamis is more important than lake height for capturing tsunamis in the lake sediments. This may also explain why there is no erosional unconformity in SAQ21-06.

4.4 Diatoms

All prepared diatom microscope slides were screened to find marine diatom species that do not normally live in freshwater systems and thus could be used as an indicator for marine water invasion. Diatom assemblages in the samples included species that typically inhabit freshwater and weakly brackish systems. Most common species that were found in almost all the samples were *Navicula vulpina*, *Navicula similis*, *Neidium iridis*, *Stauroneis phoenicenteron*, and *Tabellaria flocculosa*. Only one sample (from 61-62 cm depth) in core SAQ21-06 included diatoms that are marine origin. This sample was taken from the massive sand layer in the base of the T1 deposit, and included diatom species, *Cocconeis scutellum*, which is a common species in marine and brackish coastal waters (Cremer 1998; Witkowski et al., 2000; Pearce et al., 2014; Oksman et al., 2022).

4.5 Radiocarbon chronology

The tsunami units (T1 and T2) are present in two cores (SAQ21-06 and SAQ21-09) and combined with the absence of tsunami deposits in cores from two other lakes (SAQ21-07 and SAQ21-11) we constrain the age of the two tsunami using radiocarbon dating of macrofossils and bulk sediment (Table 1).

Samples for radiocarbon dating of T2 were taken below and above the tsunami sediments in SAQ21-06. The bulk dates below are 8.1 and 7.9 cal. ka BP and the bulk date above 7.9 cal. ka BP suggesting an age of T2 of around 7.9 cal. ka BP. However, a macrofossil (aquatic moss) sampled at the top of T2 yields an age of 7.6 cal. ka BP indicating the T2 is younger than the 7.9 cal. ka BP that the bulk sediment samples bracketing T2 yield. We suggest that the small discrepancy between the macrofossil (aquatic moss) date at the top of T2 and the bulk date above T2 is due to the re-sedimentation of older carbon in the bulk dates that makes them a few hundred years too old ages This is attributed to erosion of older organic material by the tsunami and the

subsequent redeposition into the lake as the older organic material is washed back into the lake after the tsunami event (Bondevik et al., 1997b). In core SAQ21-06 the 42 cm long sequence of laminated gyttja between T1 and T2 dates 7.9 cal. ka BP at the bottom and 7.2 cal. ka BP at the top, respectively above T2 and below T1. This combined with the close grouping of ages in and around the T2 unit in cores SAQ21-06 and -09, indicates that some of the moss and bulk sediment samples are a few hundred years too old probably because of a local reservoir effect (Marty and Myrbo, 2014; Strunk et al., 2020) and re-mobilization of old organic material by the tsunami (c.f. Bondevik et al., 1997b). Accordingly, we conclude that T2 occurred around 7.6 cal. ka BP as this is the youngest age related to T2.

A bulk sediment sample below the erosional unconformity of T1 in SAQ21-06 yields a maximum age of 7.2 cal. ka BP. Above T1 are two dates yielding ages of 5.8 and 6.7 cal. ka BP i.e. T1 seems to have occurred between 7.2 and 6.7 cal. ka BP. The oldest of the two dates, 6.7 cal. ka BP, is taken immediately above the T1 unit, while 5.8 cal. ka BP date is sampled cm above T1 and may be less affected by re-sedimentation of older sediments washing into the lakes from the surroundings after the tsunami has occurred (Bondevik et al., 1997b). However, in a nearby lake at lower elevation (SAQ21-07, 19 m a.s.l.) the sedimentary record shows continuous deposition of lacustrine sediments extending back to 7.3 cal. ka BP without any evidence of T1. To explain this discrepency we see two possibilities. Either T1 is not a tsunami deposit but a local phenomenon or something is wrong with the dating of T1. As T1 is recorded in two lakes (SAQ21-09 and 06) and is stratigraphically consistent it is not likely that it represents a slumping event or another local sedimentological phenomenon and we interpret it as a tsunami deposit. Instead, we suggest that T1 must have occurred at c. 7.3 ca. ka BP (within the uncertainty of the ^{14}C ages) to satisfy the chronology in both SAQ21-06 and -07.

5 Discussion

We consider that the topographical setting, the relative sea level history, and the age of the events, in addition to the signatures for tsunami sediment facies in lakes used by Bondevik et al. (1997a), are helpful in evaluating possible depositional processes. For example, the topographical setting of the lake basins makes it impossible for flash flooding from rainstorms and glacial meltwater to reach the lakes (Fig. 2.), and these processes cannot explain the lake stratigraphy. Earthquakes can cause slumping in the lake sediments; however, West Greenland is considered tectonically stable with minimal active faulting (Voss et al., 2007) and the geometry and succession of the sediment facies do not suggest that slumping from the lake sides has occurred. Lake inundation by tsunami waves is the remaining depositional process that can explain the presence of sediments with the stratigraphical signatures of the deposits identified here. In the following, we use the minimum run-up heights as a tool to assess the source and magnitude of the tsunami-triggering mechanism.

5.1 Tsunami run-up heights and magnitude

Our results show that at least two tsunamis T1 and T2 invaded the lakes at Saqqaq at c. 7.3 and 7.6 cal. ka BP, respectively (Fig. 5). We use the recalibrated RSL curve from Long et al. (1999) to plot the two events on curves showing the elevation of the lakes relative to the sea surface over time since deglaciation (Fig. 6). The older tsunami (T2) entered lake SAQ21-09 in 7.6 cal. ka BP when the lake had a minimum sill height of 41 m. Lake SAQ21-11, which is located 700 m further inland, has no evidence of tsunami deposits since 8.5 cal. ka BP. It had then a minimum sill height of 66 m. The bracket of minimum and maximum run-up height of tsunami T2 is thus 41-66 m (Fig 7). T2 is also recorded in lake SAQ21-06 which at the time had a minimum sill height of 21 m.

When the younger tsunami (T1) entered lake SAQ21-09 at 7.3 ka BP, the lake had a minimum sill height of 45 m marking the minimum run-up height. Like for T2, the maximum run-up height for T1 is also constrained by lake SAQ21-11 which at the time had a minimum sill height of 70 m. This brackets the run-up height of T1 to 45-70 m. T1 is also recorded in lake SAQ21-06 which had at the time had a minimum sill height of 25 m.

The absence of traces of tsunamis in the recorded lake stratigraphy in lake SAQ21-11 does not preclude that the lake was invaded by T1 and T2, as a tsunami wave loses energy as it moves inland and may leave no trace in the sedimentological record. It does, however, provide an upper bound on elevation where the tsunami was able to leave its signature in the stratigraphy.

5.2 Triggering mechanism of the tsunamis

Fig. 7 illustrates that 41 m is the minimum run-up height for any tsunami found in this study and we use this elevation to evaluate potential tsunami triggering mechanisms. Several mechanisms exist that can produce tsunamis in a setting such as Saqqaq, such as calving from glaciers, rolling icebergs, wave run-up during storms, earthquakes, and marine-terminating landslides.

Calving from glacier fronts or capsizing icebergs can generate tsunamis. MacAyeal et al. (2011) suggested that as a rule, the open-water upper limit to tsunami wave height from such a calving or capsizing event is $0.01H$, where H is the initial vertical dimension of the iceberg. Between 7 and 8 ka ago the calving fronts of the marine terminating outlet glaciers draining the ice sheet into Disko Bugt (Qeqertarsuaq) would have been located roughly where they are today (Weidick and Bennike, 2007), and the icebergs would have had to travel 45 km through the fjords of Kangia (Jakobshavn Isfjord) or Torsukattak before entering Disko Bugt itself (Fig. 8). The maximum water depth at the mouths of the two fjords would have been 280 m (Kangia) and 380 m (Torsukattak) at 8 cal. ka BP restricting the vertical height of the icebergs to less than 400 m and consequently a

theoretical upper limit of the open-water tsunami wave height to c. 4 m. A typical depth at the bottom of the Torsukattak fjord is 650 m, thus a tsunami initiated from calving would have an upper limit to wave height of c. 7 m, which would dissipate during the 65 km travel to Saqqaq (Fig. 8). Even though we do not consider the amplification of the wave heights as they near the shoreline, ice calving and capsizing icebergs do not have the ability to create waves with a run-up height of 41 m.

The wave climate in Disko Bugt is driven by a combination of locally generated wind waves and swells from the Davis Strait. The fetch for wave generation is limited, except towards the Davis Strait in south-westerly direction. Storms mostly occur during winter when sea ice at the coast limits almost all wave activity. During the sea ice free period, katabatic winds blow off the ice sheet from the east where fetch is limited. Consequently, wave run-up height is much less than the minimum found in any lake.

Earthquakes also has the potential to produce tsunamis. However West Greenland is situated on a tectonically passive continental margin and is considered tectonically stable (Voss et al., 2007).

Subaerial marine terminating landslides have the potential to produce very large run-up tsunamis in confined fjord settings (e.g., Dahl-Jensen et al., 2004; Sepulveda et al., 2010; Higman et al., 2018; Svennevig et al., 2020). The 1958 Lituya Bay landslide tsunami is the largest such tsunami recorded in historical times with a near field (c. 1.5 km from the source) maximum run-up height of 524 m (Franco et al., 2020) demonstrating the extreme tsunamigenic potential of landslides. Svennevig (2019) mapped several landslides in Vaigat strait and Pedersen et al. (2002) and Dahl-Jensen et al. (2004) marked Vaigat strait as an area where the bedrock configuration precondition landslides (Fig. 8). Svennevig et al. (2023b) found that at least nine very large post glacial rock avalanches deposits are present on the seafloor of Vaigat as little as 15 km from Saqqaq and argue, based on morphology along with the large volume and long runout, that these had a significant tsunamigenic potential.

Based on the high run-up heights and the presence of at least nine giant rock avalanches in Vaigat, we conclude that the tsunamis T1 and T2 recorded in our study were initiated by subaerial landslides entering the sea in the Vaigat strait.

5.3 Magnitude estimates of the tsunamigenic landslides

We cannot, based on the available data, pinpoint which specific landslides triggered the tsunamis we have reconstructed from the lake sediments. However, based on our estimated minimum and maximum run-up heights and the minimum and maximum distance to the largest landslides in the Vaigat strait (from Svennevig et al 2023b) we can assess the landslide volumes involved using the semi-empirical SPLASH equation (Oppikofer et al., 2018). The SPLASH equation is a parametrization of a power-law relationship between landslide volume, distance, and vertical run-up of the tsunami wave. Parameters were found by least-

squares fitting data from a limited number of large rock slope failures and the observed run-up at different distances from each landslide. It provides a semi-empirical prediction of run-up height from intended for preliminary regional studies. We use it here since it provides an estimate of the magnitude without using more advanced tsunami models which is beyond the scope of the present paper.

The distance to the giant landslides in the Vaigat strait (where they entered the sea) is 90 to 25 km (Fig. 8) and the run-ups for T1 is 45-70 m and T2 is 41-66 m as presented above (Fig. 7). Applying these numbers to the SPLASH equation we get that a landslide initiated 90 km away would have had a volume of 1.8 to 3.9 km^3 to produce the tsunami T1 and 1.5 to 3.3 km^3 to produce the tsunami T2. A landslide at the closest giant landslide deposit, just across Vaigat strait, 25 km to the southwest of Saqqaq (Fig. 8), would have had a volume of 0.34 to 0.74 km^3 to produce the tsunami T1 and 0.27 to 0.63 km^3 to produce the tsunami T2.

Svennevig et al. (2023b) calculate volumes of the three largest giant postglacial landslides in Vaigat strait (that may represent several events) to be c. 1.7 to 8.4 km^3. The largest of these: the Ujarrassusuk rock avalanche complex is situated 25 km from Saqqaq just across the strait. Had this rock avalanche occurred in a single event, a run-up height of 280 m would be expected in Vaigat strait (also using SPLASH, Oppikofer et al., 2018).

This is significantly different from the up to 0.74 km^3 we infer above for the highest possible tsunami (T1). From the nine postglacial rock avalanche complexes described by Svennevig et al. (2023b), we would expect more evidence of tsunami activity than the two events (T1 and T2) reported above and significantly higher waves. As our study does not cover the age interval from deglaciation at 10 cal. ka BP to 8.5 cal. ka BP, it is possible that deposits from the inferred multiple larger tsunamis are present in the tsunami probability field bracketed by these ages (Fig. 7).

Two recent landslide-triggered tsunamis have been observed in Vaigat strait, 1952 and in 2000. Both landslides originated from the slopes at the Nuussuaq Peninsula, the same coast Saqqaq is located. In 1952 after the Niiortuut landslide, a volume between 1.8 and 4.5 $\times 10^6$ m^3 (0.0018-0.0045 km^3) entered the sea and caused an estimated run-up in Saqqaq between 1 and 1.8 m (Svennevig et al., 2023a). During the 2000 Paatuut landslide 30 $\times 10^6$ m^3 (0.03 km^3) entered the sea (Dahl-Jensen et al., 2004) and triggered a tsunami that had a run-up of 3 m in Saqqaq (Fig. 3). Residents reported ‘strange waves’ for 2.5 hours. The location of the landslide and the duration of the wave run-up indicate multiple reflections off the steep slopes of the Vaigat strait. We conclude the T1 and T2 tsunamis also had an area of origin in the Vaigat strait. However, the historical landslides in Vaigat in 1952 and 2000 were at least an order of magnitude smaller than those that produced the T1 and T2 tsunamis we find in the lake sediment cores. We also note that there is a tsunami probability field of relatively large young tsunamis with a run-up of up to 19 m younger than 6 ka BP (Fig. 7). Constraining events in the two tsunami probability fields should be the priority of future studies.

With an increasing elevation and distance to the shore, landward lakes are expected to capture fewer and thinner sand beds, with a decreasing grain size (Bondevik et al., 1997a). The sampled lakes are at different elevations with varying exposure to reflected tsunami waves. Lakes SAQ21-09 and SAQ21-11 are far more exposed to direct waves coming from Vaigat strait than SAQ21-06 and SAQ21-07, and a landslide-tsunami reaching the latter two lakes would either must wash over the Saqqaq foreland or reflect off the northern coast of Disko Island before reaching Saqqaq (Figs. 2 and 8). However, eyewitness accounts and videos from the 2017 Karrat fjord landslide tsunami show the complexity of waves reflected, refracted, and diffracted in a fjord, especially when sea-ice is present (Paris et al., 2019). The first wave does not necessarily have the highest amplitude and waves can come from multiple directions. Therefore, at the Saqqaq foreland, the exposure of lakes to tsunami waves coming from Vaigat strait can be controlled either by the landward distance and elevation or by the exposure of lakes on the western side of the foreland. Potentially, for every tsunami, waves are captured by each lake at the Saqqaq foreland.

5.4 Implications for other records of tsunamigenic lake sediments in Disko Bugt

Other tsunami deposits have been found in lakes surrounding Disko Bugt. At Vaskebugt, Arveprinsen Ejland (Fig. 8), Long et al. (2015) re-appraise two lake cores used for basin isolation dating in a previous study (Long et al., 1999) and propose that tsunamis generated by rolling icebergs could have deposited sediments in some of the lakes. The lakes have an ideal setting for capturing tsunamis, and cores V1 and V8 may contain tsunami deposits that previously have been interpreted as internal slumping in the lakes (Long et al., 2015). Of particular interest is the tsunami unit in core V1, which is a 0.5-2 cm thick unit of coarse sand and angular gravel with an erosive base. It is enclosed in freshwater gyttja, however in some instances it directly overlies the marine sediments, resembling the tsunami sediments described by Bondevik et al. (1997a). Presently, the sill height of lake V1 is 61 m a.s.l. and would have been located at 0 m a.s.l. at 9.5 cal. ka BP (Fig. 6). The amount of erosion is unknown, but the tsunami must have occurred after 9.5 cal. ka BP. The lack of absolute age control on the tsunami facies limits the use of sill heights for discrimination between tsunamigenic mechanisms, but if for example, the tsunami had occurred 500 years after basin isolation – at 9 cal. ka BP - the lake would have risen to a sill height of 11 m a.s.l., which would exclude rolling icebergs as the tsunamigenic mechanism based on the arguments discussed above in section 5.2. Lake V8 is also located at Vaskebugt and presently has a sill height of c. 13 m and a modelled age of isolation of 6.7 cal. ka BP. It is suggested by Long et al. (2015) that the potential tsunami unit in this lake could represent a marine flooding of the lake basin and adjoining surfaces. The V8 radiocarbon sample (5.2 cal. ka BP) appears not to have been sampled at the marine contact, but above the tsunami facies and it is excluded from the RSL reconstruction in both Long et al. (1999) and the present study (Fig. 4). Thus, the tsunami responsible for the tsunami facies in lake V8 should have occurred between 6.7 and 5.2 cal. ka BP when the sill heights were between 0 m and 12 m a.s.l. This is inside the younger tsunami possibility field (Fig. 7) and both landslides and rolling icebergs could have been the mechanism initiating the tsunami.

Long et al. (2015) also describe a likely tsunami deposit in lake IV4 at Tasiusarsuit in the southern part of Disko Bugt (Fig. 8) and attribute it to an iceberg generated tsunami occurring at 6.1 cal. ka BP (6242–5910 cal. ka BP). This single event is recorded in lake IV4 in the 200-year window where the estimated >3 m run-up height from an iceberg generated wave was able to reach the lake. The interpretation that icebergs generated the waves that entered the lakes at Tasiusarsuit and Vaskebugt relies on a topographical analysis and the then current knowledge of landslide- and iceberg generated tsunamis in Disko Bugt (Long et al., 2015). An important assumption made by Long et al. (2015) is that the 2000 Paatuut landslide is the largest tsunamigenic landslide that is likely to occur in Vaigat strait, and due to large distances from areas with a high frequency of landslides in Vaigat strait and the south coast of Disko Island, the wave energy would have dissipated before reaching the lakes at Vaskebugt or Tasiusarsuit. Landslide tsunamis may also have reached lake IV at Tasiusarsuit from the south coast of Disko Island where Svennevig (2019) mapped giant landslides (Fig. 8). However, the seafloor off the south coast of Disko Island has only few depth soundings (Morlighem et al., 2021), and no presence of submarine landslide landforms has been reported.

The present study shows that there is onshore evidence of giant landslide-generated tsunamis in the Vaigat strait, and these could have reached Vaskebugt and explain the presence of the tsunami units in lakes V1 and V8. The age control of these units is not of sufficient quality to unambiguously explain if these deposits were generated by waves from landslides or rolling icebergs.

Identifying additional tsunamis and constraining their timing are outstanding research questions, and the scientific literature on lake deposits (i.e., Long et al., 2015) and gaps in the bathymetric data indicates that this will be revealed by conducting additional offshore and onshore research in the Vaigat strait and Disko Bugt areas, as well as additional field work in the lakes around Saqqaq could reveal more tsunami deposits and provide better identification and improved age control over tsunamis that are reported here.

6 Conclusion

We analysed lake sediment cores from the Saqqaq foreland in West Greenland and found sediments that we interpret to be deposited by tsunamis. We can distinguish between at least two tsunami events (T1: 7.3 and T2: 7.6 cal. ka BP), each with multiple waves, and determine minimum run-up heights of 45 and 41 m, respectively. We find no tsunami deposits in a higher elevation which helps us constrain the maximum possible run-up height to 70 and 66 m. Due to the large run-up heights, and the presence of deposits from giant rock avalanches in the Vaigat strait 25 to 90 km from Saqqaq we conclude that the tsunamis were likely triggered by giant landslides.

Two historic landslide-triggered tsunamis in 1952 and 2000 had run-up heights of 1-1.8 m and 3 m in Saqqaq, respectively, shows that historic events are at least an order of magnitude smaller than T1 and T2. However, tsunamis with a run-up height of up to 19 m could have occurred in the past 6000 years without being captured in the cored lakes as this interval is not covered by our survey. Likewise, the time between our oldest dated sediment core bottom (8.5 ka BP) and deglaciation (10 ka BP) defines a possibility field where older giant landslide tsunamis could have occurred. Nine giga-scale landslide deposits are described from Vaigat strait and as we only identify deposits from two resulting tsunamis in our study, we infer that the deposits from these other landslides could be encountered in this possibility field.

Data availability

XRF core scanning data and AMS radiocarbon certificates are available at the GEUS Dataverse (currently shared using a private link, but will be publicly available when manuscript has been issued final doi):
https://dataverse.geus.dk/privateurl.xhtml?token=a64a3df7-add2-49e7-868d-2512becb62df

CrediT authorship statement

Niels Jákup Korsgaard: Conceptualization; Formal analysis; Investigation – field work lead and laboratory work; Visualization; Writing – original draft preparation. Kristian Svennevig: Conceptualization; Formal analysis; Investigation – field work; Visualization; Writing – review & editing. Anne Sofie Søndergaard: Investigation – field work; Formal analysis; Visualization; Writing – review & editing. Gregor Luetzenburg: Investigation – field work; Writing – review and editing. Mimmi Oksman: Investigation – microfossil screening; Formal analysis; Writing – review & editing. Nicolaj Krog Larsen: Resources – field equipment & laboratory facilities; Writing – review & editing.

Competing interests

The authors declare that they have no conflict of interest.

Acknowledgements

We thank Anthony Henry Ruter for identification of radiocarbon samples and Marie-Louise Siggaard-Andersen for XRF laboratory work. Anders Schomacker is thanked for constructive comments on the manuscript and K. Pauli for general support.

References

SDFI (Agency for Data Supply and Infrastructure): Grønlandske pilotdata - Disko Bugt [DEM] [ORTOFOTO] [TOPO50], https://dataforsyningen.dk/data/4516, [Accessed 28/06/2018].

Battarbee, R.W., Jones, V.J., Flower, R.J., Cameron, N. G., Bennion, H., Carvalho, L., and Juggins, S.: Diatoms, in: Tracking Environmental Change Using Lake Sediments Volume 3, Terrestial, Algal, and Siliceous Indicators, edited by: Smol, J.P., Birks, H.J.B., and Last, W.M., Kluwer Academic Publishers, Dordrecht, Netherlands, 155–202, https://doi.org/10.1007/0-306-47668-1, 2001

Blikra, L.H., Longva, O., Braathen, A., Dehls, J.F., Stalsberg, K., and Anda, E.: Rock slope failures in Norwegian fjord areas: Examples, spatial distribution and temporal pattern, In: Evans, S.G., Mugnozza, G.S., Strom, A., Hermanns, R.L. (eds.) Landslides from Massive Rock Slope Failure. NATO Science Series, vol 49. Springer, Dordrecht. https://doi.org/10.1007/978-1-4020-4037-5_26, 2006.

Bondevik S, Svendsen, J.I., Mangerud, J.: Tsunami sedimentary facies deposited by the Storegga tsunami in shallow marine basins and coastal lakes, western Norway. *Sedimentology* 44, 1115-1131, https://doi.org/10.1046/j.1365-3091.1997.d01-63.x, 1997a.

Bondevik, S., Svendsen, J. I., Johnsen, G., Mangerud, J. & Kaland, P. E.: The Storegga tsunami along the Norwegian coast, its age and runup. *Boreas* 26, 29-53, https://doi.org/10.1111/j.1502-3885.1997.tb00649.x, 1997b.

Bronk Ramsey, C.: Bayesian analysis of radiocarbon dates. Radiocarbon 51, 337–360, https://doi.org/10.1017/S0033822200033865, 2009.

Chagué-Goff, C., Szczuciński, W., and Shinozaki, T.: Applications of geochemistry in tsunami research: A review. *Earth-Sci Rev.* 165, 203-244, https://doi.org/10.1016/j.earscirev.2016.12.003, 2017.

Coeurdevey, L. and Soubirane, J.: SPOT 6/7 Imagery – User Guide, Technical Reference, Report No. SI/DC/13034-v1.0, Airbus Defence and Space Intelligence, France, 1-62, https://earth.esa.int/eogateway/documents/20142/37627/SPOT-6-7-imagery-user-guide.pdf, 2013.

Cremer, H.: The diatom flora of the Laptev Sea (Arctic Ocean). Bibliotheca Diatomologica Bd. 40, J. Cramer, Berlin & Stuttgart, 1998.

Dahl-Jensen, T., Larsen L. M., Pedersen, S. A. S., Pedersen, J., Jepsen, H. F., Pedersen, G., Nielsen, T., Pedersen, A. K., von Platen-Hallermund, F., and Weng, W.: Landslide and Tsunami 21 November 2000 in Paatuut, West Greenland, *Nat. Hazards* 31: 277–287, https://doi.org/10.1023/B:NHAZ.0000020264.70048.95, 2004.

Dam, G., Krarup Pedersen, G., Sønderholm, M., Midtgaard, H. H., Melchior Larsen, L., Nøhr-Hansen, H., and Pedersen, A. K.: Lithostratigraphy of the Cretaceous–Paleocene Nuussuaq Group, Nuussuaq Basin, West Greenland. *GEUS Bulletin*, 19, 1–171. https://doi.org/10.34194/geusb.v19.4886, 2009.

Franco, A., Moernaut, J., Schneider-Muntau, B., Strasser, M., and Gems, B.: The 1958 Lituya Bay tsunami - Pre-event bathymetry reconstruction and 3D numerical modelling utilising the computational fluid dynamics software Flow-3D: *Nat. Hazards Earth Syst. Sci.*. 20, 2255–2279, https://doi.org/10.5194/nhess-20-2255-2020, 2020.

Garde, A. and Steenfelt, A.: *Precambrian geology between Qarajaq Isfjord and Jakobshavn Isfjord, West Greenland 1: 250,000*. *Grønlands Geologiske Undersøgelse*, 1994.

GRASS Development Team: Geographic Resources Analysis Support System (GRASS) Software, Version 8.0. *Open Source Geospatial Foundation*. https://grass.osgeo.org, 2022.

Heaton, T.J., Kohler, P., Butzin, M., Bard, E., Reimer, R.W., Austin, W.E.N., Bronk Ramsey, C., Grootes, P.M., Hughen, K.A., Kromer, B., Reimer, P.J., Adkins, J., Burke, A., Cook, M.S., Olsen, J., and Skinner, L.C.: Marine20 - the marine radiocarbon age calibration curve (0-55,000 cal Bp). *Radiocarbon* 62, 779-820, https://doi.org/10.1017/RDC.2020.68, 2020.

Hermanns, R.L., L'heureux, J.S., and Blikra, L.H.: Landslide triggered tsunami, displacement wave, Encyclopedia of Earth Sciences Series, 611–615, https://doi.org/10.1007/978-1-4020-4399-4_95, 2013.

Hermanns, R.L., Penna, I.M., Oppikofer, T., Noël, F., and Velardi, G.: Rock Avalanche, Shroder, J.F. (ed.), Treatise on Geomorphology, Elsevier, https://doi.org/10.1016/B978-0-12-818234-5.00183-8, 2021.

Higman, B., Shugar, D.H., Stark, C.P., Ekström, G., Koppes, M.N., Lynett, P., Dufresne, A., Haeussler, P.J., Geertsema, M., Gulick, S., Mattox, A., Venditti, J.G., Walton, M.A.L., McCall, N., Mckittrick, E., MacInnes, B., Bilderback, E.L., Tang H., Willis, M.J., Richmond, B., Reece, R.S., Larsen, C., Olson, B., Capra, J., Ayca, A., Bloom, C., Williams, H., Bonno, D., Weiss, R., Keen, A., Skanavis, V., and Loso, M.: The 2015 landslide and tsunami in Taan Fiord, Alaska: *Sci. Rep.* 8, 1–13, https://doi.org/10.1038/s41598-018-30475-w, 2018.

Hungr, O., Leroueil, S., and Picarelli, L.: The Varnes classification of landslide types, an update. *Landslides* 11, 167–194, https://doi.org/10.1007/s10346-013-0436-y, 2014.

Long, A.J., Roberts, D.H., and Wright, M.R.: Isolation basin stratigraphy and Holocene relative sea-level change on Arveprinsen Ejland, Disko Bugt, West Greenland. *J. Quat. Sci*. 14 (4) 323–345, doi.org/10.1002/(SICI)1099-1417(199907)14:4%3C323::AID-JQS442%3E3.0.CO;2-0, 1999.

Long, A.J., Roberts D.H., Simpson, M.J.R., Dawson, S., Milne, G.A., and Huybrechts, P.: Late Weichselian relative sea-level changes and ice sheet history in southeast Greenland. Earth Plan Sci Letts 8(2) 8-18, https://doi.org/10.1016/j.epsl.2008.03.042,2008.

Long, A.J., Szczuciński, W., and Lawrence. T.: Sedimentary evidence for a mid-Holocene iceberg-generated tsunami in a coastal lake, west Greenland. *Arktos* 1:6, https://doi.org/10.1007/s41063-015-0007-7, 2015.

MacAyeal, D.R., Abbot, D.S. and Sergienko, O.V.: *Ann. of Glaciol.* 52, 58, 51–56, https://doi.org/10.3189/172756411797252103, 2011.

Marty J. and Myrbo, A.: Radiocarbon dating suitability of aquatic plant macrofossils. *J Paleolimnol* 52:435–443, https://doi.org/10.1007/s10933-014-9796-0, 2014.

Marcussen, C., Chalmers, J.A., Andersen, H.L., Rasmussen R. and Dahl-Jensen, T.: Acquisition of high-resolution multichannel seismic data in the offshore part of the Nuussuaq Basin, central West Greenland. *Geology of Greenland Survey Bulletin* 189, 34–40, https://doi.org/10.34194/ggub.v189.5195, 2001.

Morlighem, M., Williams, C. N., Rignot, E. J., An, L., Arndt, J. E., Bamber, J. L., Catania, G. A., Chauché, N., Dowdeswell, J. A., Dorschel, B., Fenty, I., Hogan, K., Howat, I. M., Hubbard, A. L., Jakobsson, M., Jordan, T. M., Kjeldsen, K. K., Millan, R., Mayer, L., Mouginot, J., Noël, B. P. Y., O'Cofaigh, C., Palmer, S. J., Rysgaard, S., Seroussi, H., Siegert, M. J., Slabon, P., Straneo, F., Broeke, M. R. van den, Weinrebe, W., Wood, M., and Zinglersen, K. B.: IceBridge BedMachine Greenland, Version 4, NASA National Snow and Ice Data Center Distributed Active Archive Center, https://doi.org/10.5067/VLJ5YXKCNGXO, 2021.

Oksman, M., Kvorning, A.B., Larsen, S.H., Kjeldsen, K.K., Mankoff, K.D., Colgan, W., Andersen, T.J.Nørgaard-Pedersen, N., Seidenkrantz, M.-S., Mikkelsen, N., and Ribeiro, S.: Impact of freshwater runoff from the southwest Greenland Ice Sheet

on fjord productivity since the late 19th century. *The Cryosphere* 16, 2471–2491, https://doi.org/10.5194/tc-16-2471-2022, 2022.

Oppikofer, T., Hermanns, R.L., Roberts, N.J., and Böhme, M.: SPLASH: semi-empirical prediction of landslide-generated displacement wave run-up heights. Subaqueous Mass Movements, Lintern, D.G.,Mosher, D.C., Moscardelli, L.G., Bobrowsky, P.T., Campbell, C., Chaytor, J.D., Clague, J.J., Georgiopoulou, A., Lajeunesse, P., Normandeau, A., Piper, D.J.W., Scherwath, M., Stacey, C. and Turmel, D. (eds.), Geological Society, London, Special Publications 477, https://doi.org/10.1144/SP477.1, 2018.

Paris, A., Okal, E.A., Guérin, C., Heinrich, P., Schindelé, F., and Hébert, H.: Numerical Modeling of the June 17, 2017 Landslide and Tsunami Events in Karrat Fjord, West Greenland. *Pure and Applied Geophysics* 176, 3035–3057, https://doi.org/10.1007/s00024-019-02123-5, 2019.

Patton, A.I., Rathburn, S.L., and Capps, D.M.: Landslide response to climate change in permafrost regions. *Geomorphology* 340, 116–128, https://doi.org/10.1016/j.geomorph.2019.04.029, 2019.

Pearce, C., Weckström, K., Sha, L., Miettinen, A., and Seidenkrantz, M.-S.: The Holocene marine diatom flora of Eastern Newfoundland bays. *Diatom Research*, 29:4, 441-454, https://doi.org/10.1080/0269249X.2014.925508, 2014.

Pearce, C., Özdemir, K. S., Forchhammer, R. C., Detlef, H., and Olsen, J.: The marine reservoir age of Greenland coastal waters, Geochronology Discuss. [preprint], https://doi.org/10.5194/gchron-2023-7, in review, 2023.

Pedersen, M., Weng, W. L., Keulen, N., and Kokfelt, T. F.: A new seamless digital 1:500 000 scale geological map of Greenland. *GEUS Bulletin*, 28, 65–68. https://doi.org/10.34194/geusb.v28.4727, 2013.

Pedersen, S.A.S., Larsen, L.M., Dahl-jensen, T., Jepsen, H.F., Krarup, G., Nielsen, T., Pedersen, A.K., von Platen-Hallermund, F., and Weng, W.L.: Tsunami-generating rock fall and landslide on the south coast of Nuussuaq, central West Greenland. *Geology of Greenland Survey Bulletin* 191, 73–83, https://doi.org/10.34194/ggub.v191.5131, 2002.

Porter, C., Morin, P., Howat, I., Noh, M.-J., Bates, B., Peterman, K., Keesey, S., Schlenk, M., Gardiner, J., Tomko, K., Willis, M., Kelleher, C., Cloutier, M., Husby, E., Foga, S., Nakamura, H., Platson, M., Wethington, M. Jr., Williamson, C., Bauer, G., Enos, J., Arnold, G., Kramer, W., Becker, P., Doshi, A., D'Souza, C., Cummens, P., Laurier, F., and Bojesen, M.: ArcticDEM, v3.0, Harvard Dataverse [data set], https://doi.org/10.7910/DVN/OHHUKH, 2018.

Pulvertaft, T.C.R.: The geology of Sarqaqdalen, west Greenland, with special reference to the Cretaceous boundary fault system. *Grønlands Geologiske Undersøgelse Open File Series* No. 89/5. 1989.

Reimer, P. J., Austin, W. E. N., Bard, E., Bayliss, A., Blackwell, P. G., Bronk Ramsey, C., Butzin, M., Cheng, H., Edwards, R.L., Friedrich, M., Grootes, P. M., Guilderson, T. P., Hajdas, I., Heaton, T. J., Hogg, A. G., Hughen, K. A., Kromer, B., Manning, S. W., Muscheler, R., Palmer, J. G., Pearson, C., van der Plicht, H., Reimer, R. W., Richards, D., Scott, E. M., Southon, J. R., Turney, C. S. M., Wacker, L., Adophi, F., Büntgen, U., Capano, M., Fahrni, S., Fogtmann-Schulz, A., Friedrich, R., Kudsk, S., Miyake, F., Olsen, J., Reinig, F., Minoru Sakamoto, M., Sookde A., and Talamo, S.: The IntCal20 Northern Hemisphere radiocar-bon calibration curve (0–55 kcal BP), *Radiocarbon*, 62, 725–757, https://doi.org/10.1017/RDC.2020.41, 2020.

Rothwell, R. and Croudace, I.: Twenty Years of XRF Core Scanning Marine Sediments: What Do Geochemical Proxies Tell Us?, in: Micro-XRF Studies of Sediment Cores. Developments in Paleoenvironmental Research, edited by: Croudace, I., Rothwell, R., Springer, Dordrecht, vol 17, 25-102, https://doi.org/10.1007/978-94-017-9849-5_2, 2015

Sepulveda, S.A., Serey, A., Lara, M., Pavez, A., and Rebolledo, S.: Landslides induced by the April 2007 Aysén Fjord earthquake, Chilean Patagonia: Landslides 7, 483–492, https://doi.org/10.1007/s10346-010-0203-2, 2010.

Shinozaki, T.: Geochemical approaches in tsunami research: current knowledge and challenges. *Geosci. Lett.* 8:6, https://doi.org/10.1186/s40562-021-00177-9, 2021.

Strunk, A., Olsen, J., Sanei, H., Rudra, A. and Larsen, N.K.: Improving the reliability of bulk sediment radiocarbon dating, *Quat. Sci. Rev.* 242, 106442, https://doi.org/10.1016/j.quascirev.2020.106442, 2020.

Svennevig, K.: Preliminary landslide mapping in Greenland. *GEUS Bulletin*, 43. https://doi.org/10.34194/GEUSB-201943-02-07, 2019.

Svennevig, K., Dahl-Jensen, T., Keiding, M., Boncori, J.P.M., Larsen, T., Salehi, S., Solgaard, A.M., and Voss, P.H.: Evolution of events before and after the 17 June 2017 rock avalanche at Karrat Fjord, West Greenland – a multidisciplinary approach to detecting and locating unstable rock slopes in a remote Arctic area: *Earth Surface Dynamics* 8, 1021–1038, https://doi.org/10.5194/esurf-8-1021-2020, 2020.

Svennevig, K., Hermanns, R.L., Keiding, M., Binder, D., Citterio, M., Dahl-Jensen, T., Mertl, S., Sørensen, E.V., and Voss, P.H.: A large frozen debris avalanche entraining warming permafrost ground - the June 2021 Assapaat landslide, West Greenland. *Landslides*, https://doi.org/10.1007/s10346-022-01922-7, 2022.

Svennevig, K., Keiding, M., Korsgaard, N.J., Lucas, A., Owen, M., Poulsen, M.D., Priebe, J., Sørensen E.V., Morino, C.: Uncovering a 70-year-old permafrost degradation induced disaster in the Arctic, the 1952 Niiortuut landslide-tsunami in central West Greenland. Science of the Total Environment, 859. https://doi.org/10.1016/j.scitotenv.2022.160110, 2023a.

Svennevig, K., Owen, M.J., Citterio, M., Nielsen, T., Rosing, S., Harff, J., Endler, R., Morlighem, M., Rignot., E. Holocene giga-scale rock avalanches in Vaigat, West Greenland – implications for geohazard. *Geology, in review*, 2023b.

Voss, P.H., Poulsen, K., Simonsen, S.B., and Gregersen, S.: Seismic hazard assessment of Greenland. *Geol. Surv. Denmark Greenl. Bull.* 13, 57–60. https://doi.org/10.34194/geusb.v13.4976, 2007.

Wagner, B., Bennike, O., Klug, M., and Cremer, H.: First indication of Storegga tsunami deposits from East Greenland. *J. of Quat. Sci.* 22, 321-325. https://doi.org/10.1002/jqs.1064, 2006.

Weidick, A.: Observations on some Holocene glacier fluctuations in West Greenland. *Bulletin Grønlands Geologiske Undersøgelse*, 73, 1–202. https://doi.org/10.34194/bullggu.v73.6611, 1968.

Weidick, A.: Holocene shore-lines and glacial stages in Greenland - an attempt at correlation. *Rapport Grønlands Geologiske Undersøgelse*, 41, 1–39. https://doi.org/10.34194/rapggu.v41.7281, 1972.

Weidick, A. and Bennike, O.: Quaternary glaciation history and glaciology of Jakobshavn Isbræ and the Disko Bugt region, West Greenland: a review. *GEUS Bulletin*, *14*, 1–78. https://doi.org/10.34194/geusb.v14.4985, 2007.

Witkowski, A., Lange-Bertalot, H., and Metzeltin, D.: Diatom flora of marine coasts I. Iconographia Diatomologica Vol. 7. A.R.G.Ganter Verlag K.G., Ruggell. 925 pp., ISBN 9783904144100, 2000.

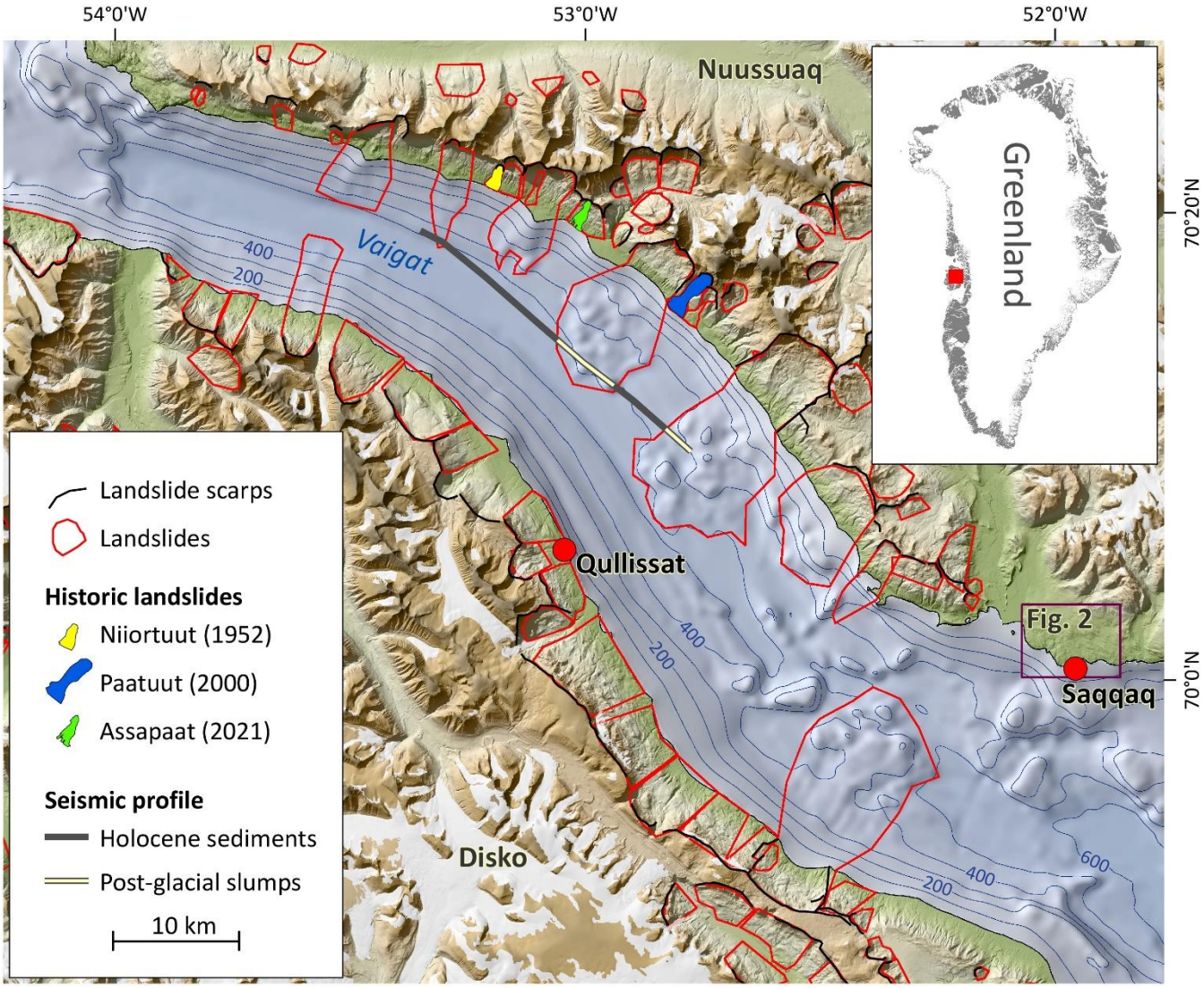

Figure 1: Landslide mapping by Svennevig (2019) and Svennevig et al (2023b). Bathymetry from Bedmachine Greenland v4 (Morlighem et al., 2021), other map data from SDFI (2018) and ArcticDEM (Porter et al., 2018). A seismic profile line from Vaigat available from Marcussen et al. (2001) is shown, where the sediments along the profile were interpreted as either post-glacial slumps or glacial moraines, surrounded by horizontal Holocene sediments.

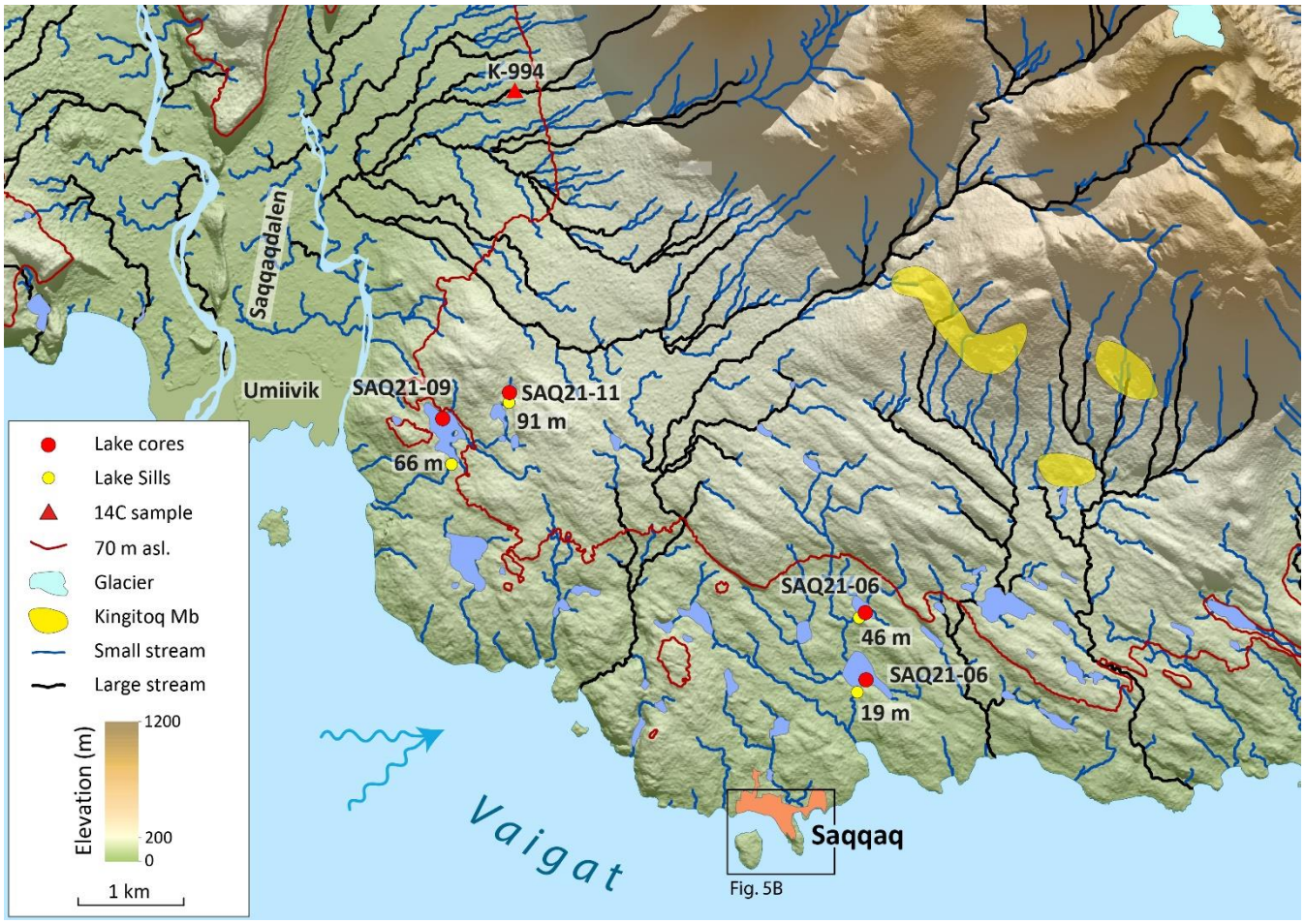

Figure 2: Lake sediment coring sites at the Saqqaq foreland and surroundings. The foreland elevation ranges 0-200 m a.s.l. and has multiple lakes in this height interval. The elevation colour scale has been partitioned into intervals below and above 200 m to emphasize the morphology. Inferred directional ranges of the tsunamis are indicated with wavy blue arrows. Catchments of the cored lakes are local and water entering the lakes is from rainfall or snowmelt and sheltered from the rivers draining the mountains. The 70 m contour represents the coastline at 10.0 ca. ka BP as inferred by a radiocarbon dated marine shell (K-994 from Weidick, 1972). DEM and map data from SDFI (2018) except for the streams which were derived from the DEM using GRASS (2022). Geological map data from Pedersen et al. (2013).

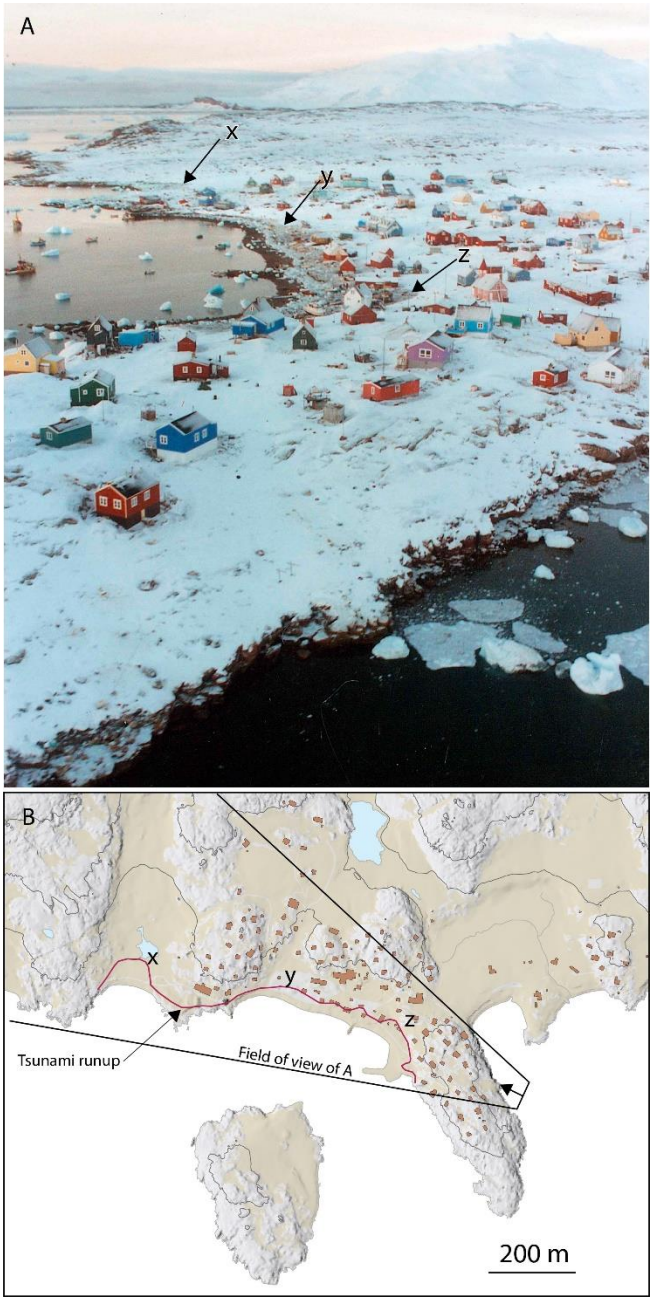

Figure 3: A) photograph by the Illulissat Police the day after the tsunami that reached Saqqaq after the November 21, 2000, landslide at Paatuut. The maximum run-up is seen as discoloration and removal of the snow indicated with x, y and z. B) Topographic map of Saqqaq from ASIAQ with the viewing direction and field of view of the photo in A. The maximum tsunami run-up is indicated with a red line x, y, and z refers to the same marked localities in A.

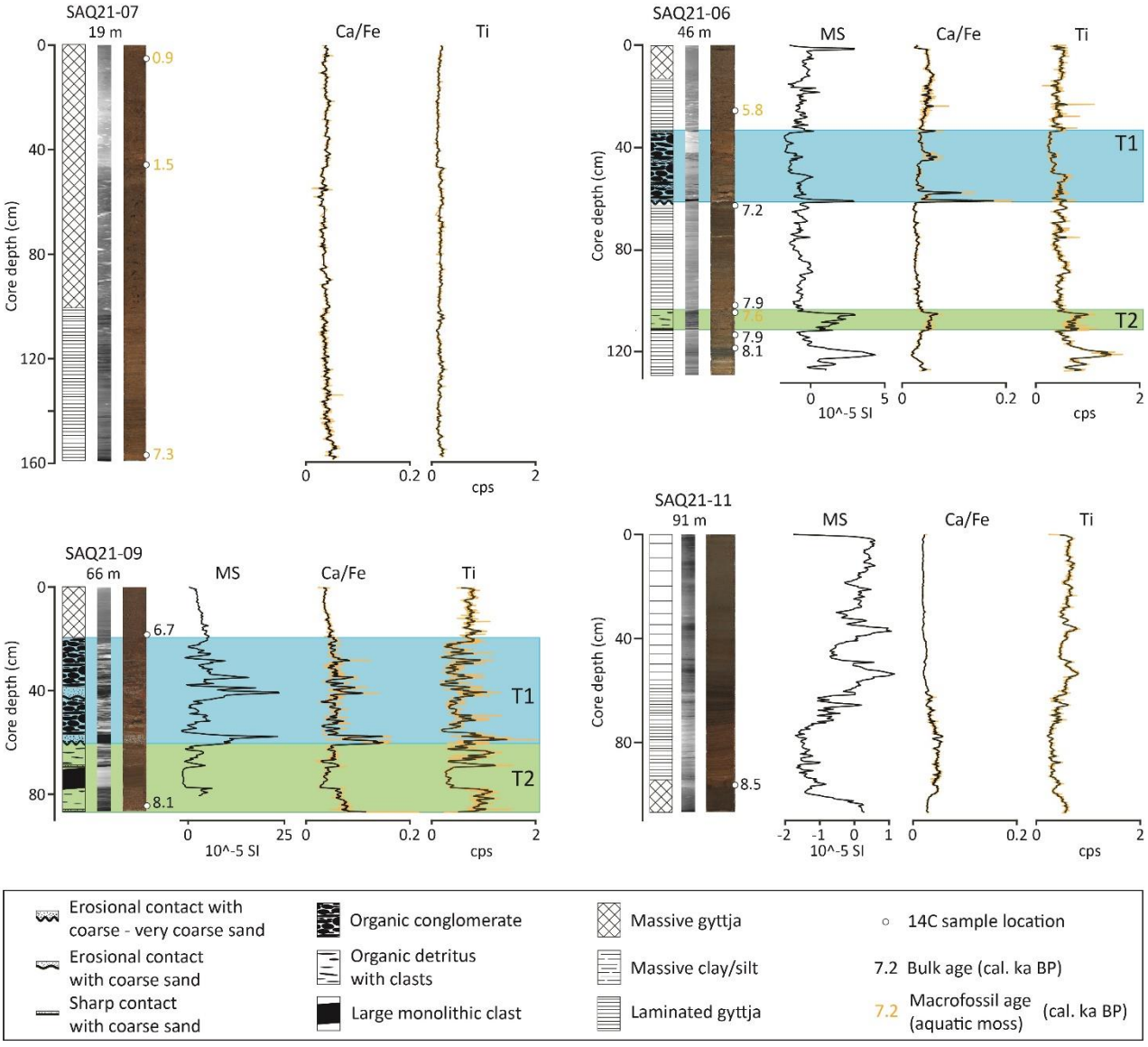

Figure 4: Sediment proxies (optical core and x-ray images, stratigraphy and XRF) and calibrated radiocarbon ages from the four lakes. T1 and T2 show tsunami sediment units.

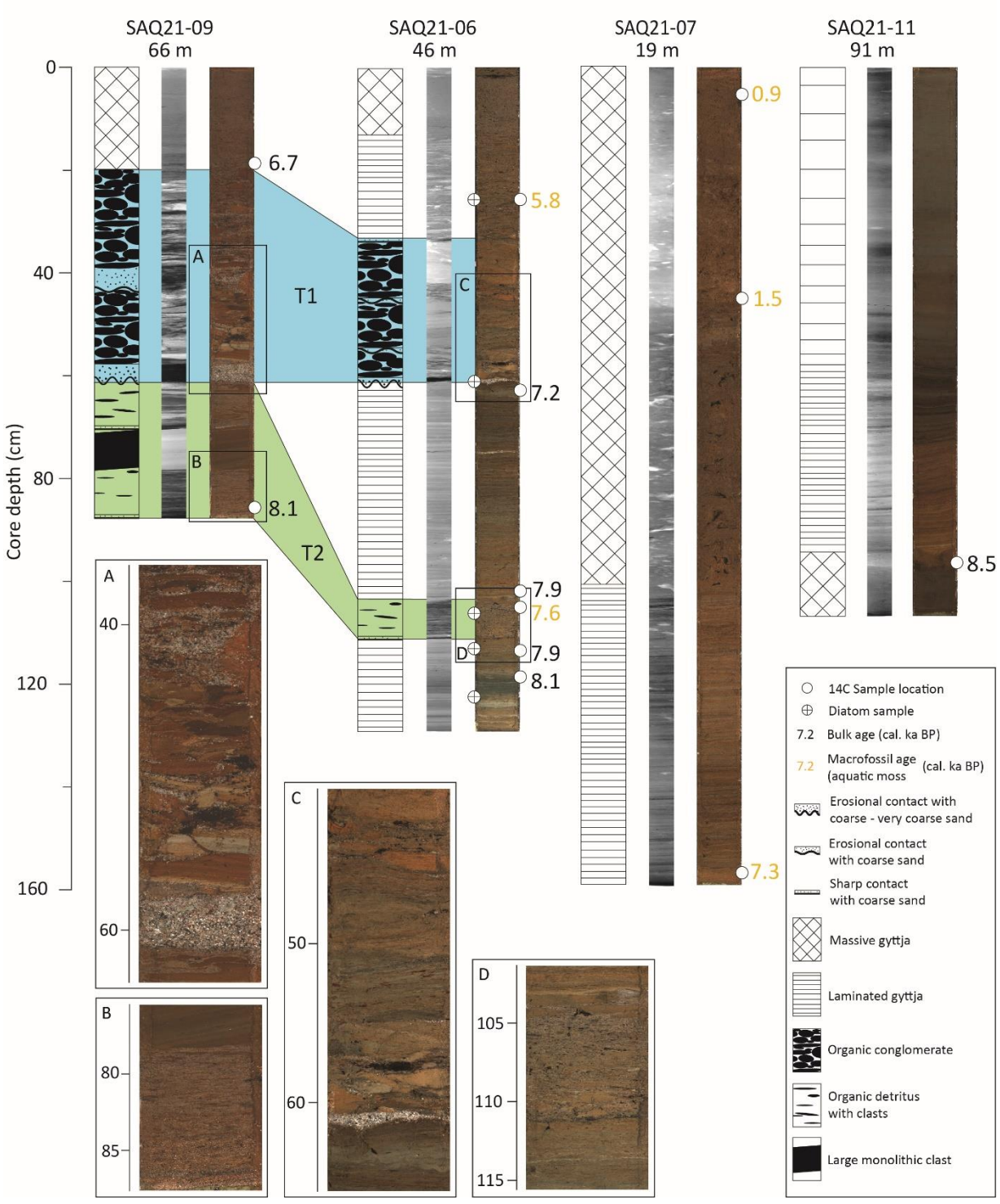

Figure 5: Correlation of tsunami facies T1 and T2 in lake cores SAQ21-06 and SAQ21-09. A-D show details of the tsunami units T1 and T2.

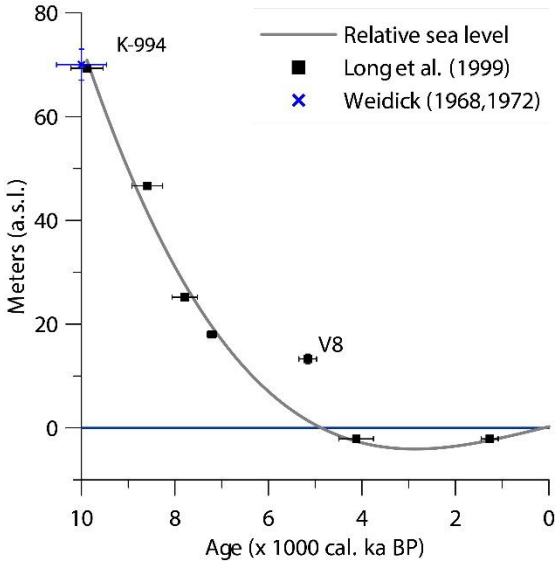

730

Figure 6: Recalibrated relative sea level curve from Vaskebugt, Arveprinsen Ejland (Long et al., 1999). Sample V8 was excluded from the polynomial fit.

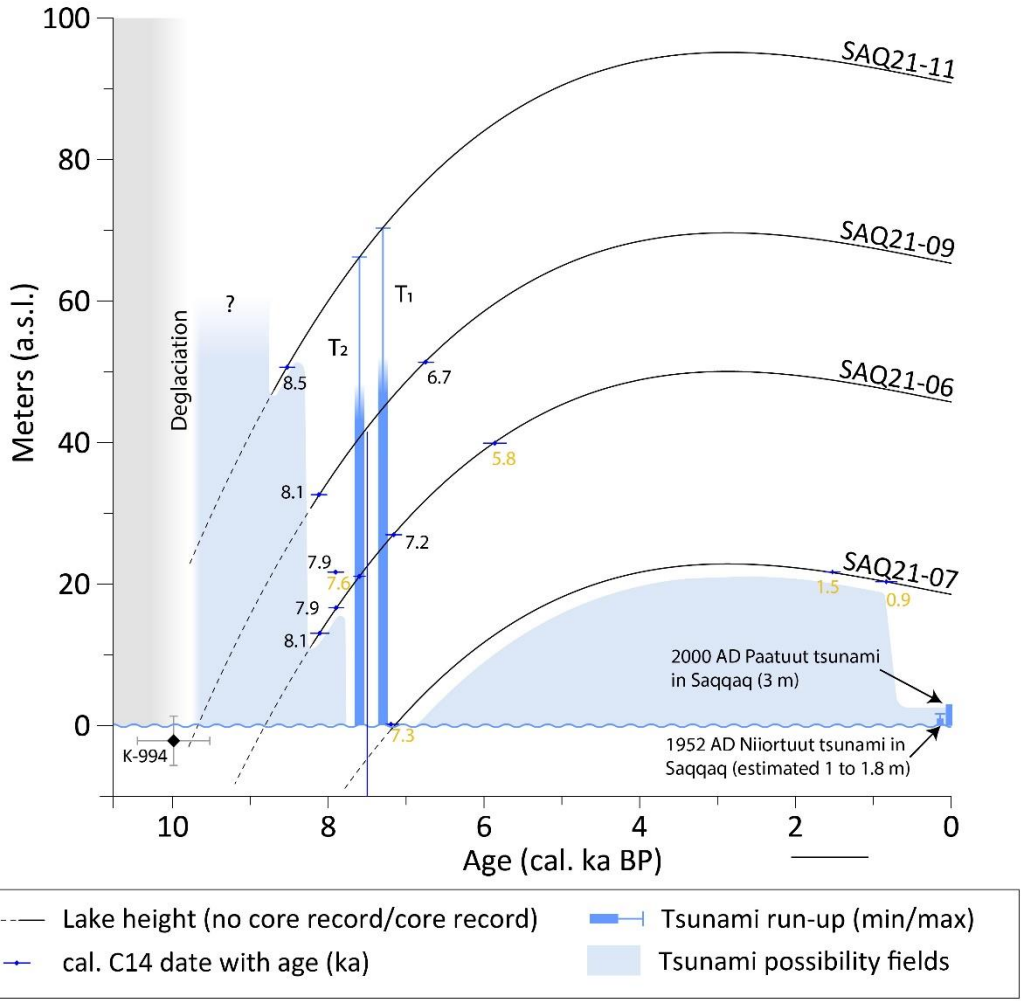

Fig. 7. Lake elevations of four lakes extended back in time using present-day elevation and the recalibrated relative sea level curve (Fig. 6). Tsunamis T1 and T2 have been plotted and the intersection with the lake elevation curves shows the lake elevations when lakes SAQ21-06 and -09 were invaded by tsunami waves. This provides the minimum run-up height of T1 and T2. There is no sediment older than 8.5 cal. ka BP in our core record, and after c. 6 cal. ka BP a tsunami would have to have a minimum run-up of up to 19 m to reach a lake. These elevations/ages define fields where tsunamis are possible, but not recorded by our data (light blue "tsunami possibility fields"). The maximum run-up heights of two historical tsunami waves from 1952 (Svennevig et al., 2023a) and 2000 from the present study are shown for comparison.

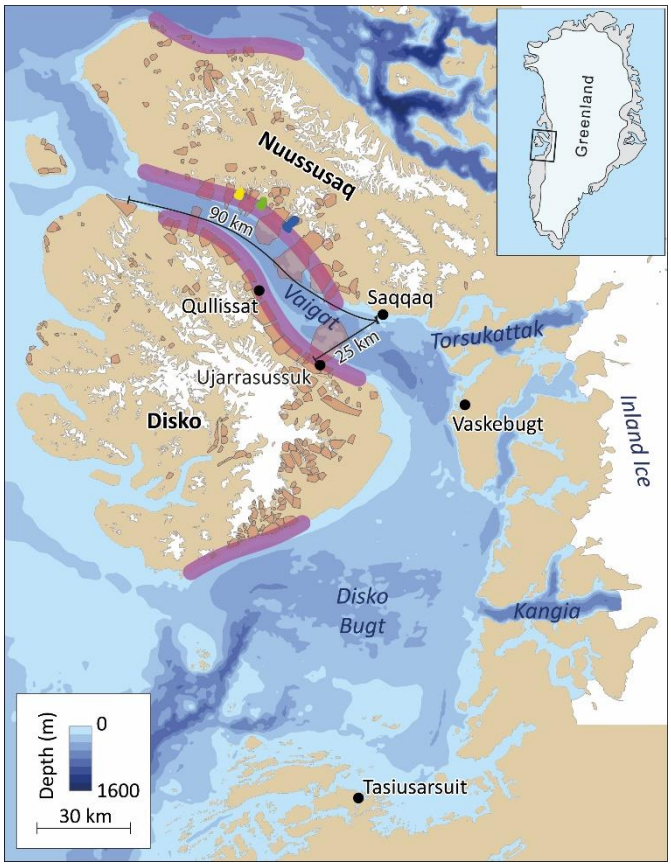

Figure 8: Bathymetry of Disko Bugt, Vaigat and neighboring fjords (Pedersen et al., 2013; Morlighem et al., 2021). Areas with a high risk of landslides (Dahl-Jensen et al., 2004) is shown as purple shadings along the north and south coasts of Disko island and Nuussuaq. Mapped post glacial landslides (Svennevig, 2019) are shown as red polygons and historical landslides in Vaigat in 1952 (Niiortuut, yellow), 2000 (Paatuut, blue), and 2021 (Assapaat, green) are also indicated.

Lab number	Core/Lake No.	Latitude °N	Longitude °W	Sample depth from core top (cm)	Material	14C age BP ± 1σ	cal. ka BP (max)	cal. ka BP (min)	Sigma	cal. ka BP (median)	Sample setting	Reference	Minimum sill height (m a.s.l.)	Sigma (m)
Ua-74363	SAQ21-06	70.026179	51.920846	26-27	Aquatic bryophytes	5024±37	5897	5658	75	5782	Above tsunami deposit	This study	46.0	1.6
Ua-74355	SAQ21-06	70.026179	51.920846	62-63	Gyttja	6315±35	7310	7164	46	7223	Below erosional unconformity	This study	46.0	1.6
Ua-74356	SAQ21-06	70.026179	51.920846	102-103	Gyttja	7081±44	8008	7795	48	7899	Above tsunami deposit	This study	46.0	1.6
Ua-74364	SAQ21-06	70.026179	51.920846	105-106	Aquatic bryophytes	6775±37	7675	7575	31	7625	Single fossil in top of tsunami deposit	This study	46.0	1.6
Ua-74357	SAQ21-06	70.026179	51.920846	112-113	Gyttja	7097±35	8008	7843	41	7929	Below erosional unconformity	This study	46.0	1.6
Ua-74358	SAQ21-06	70.026179	51.920846	118-119	Gyttja	7335±37	8281	8024	59	8110	Ti and Ca/Fe ratio shift	This study	46.0	1.6
Ua-74365	SAQ21-07	70.020487	51.920420	5.0	Aquatic bryophytes	1020±46	1054	792	63	926	Top of core	This study	18.8	1.6
Ua-74366	SAQ21-07	70.020487	51.920420	46.5	Aquatic bryophytes	1628±35	1585	1405	52	1487	Ti and Ca/Fe ratio shift	This study	18.8	1.6
Ua-74359	SAQ21-07	70.020487	51.920420	156-157	Gyttja	6412±34	7423	7267	50	7341	Bottom of core	This study	18.8	1.6
Ua-74360	SAQ21-09	70.042056	52.026509	18-19	Gyttja	5861±33	6780	6564	46	6686	Above tsunami deposit	This study	65.6	1.6
Ua-74361	SAQ21-09	70.042056	52.026509	84-85	Gyttja	7319±36	8185	8025	50	8105	Rip-up clast in tsunami sediments	This study	65.6	1.6
Ua-74362	SAQ21-11	70.044366	52.010009	95-96	Gyttja	7742±35	8591	8430	46	8512	Ti and Ca/Fe ratio shift	This study	91.1	1.6
K-994	Saqqaq, Disko Bugt	70.07	52.01	-	Shells, Hiatella Arctica	8940±170	10521	9525	256	10026	Uppermost part of marine clay	Weidick 1968, 1972	70	3
Beta-107879	V0, Arveprinsen Ejland	69.76236	51.23374	-	Gyttja	8820±100	10180	9557	171	9881	Isolation contact	Long et al., 1999	69.30	0.46
Beta-112544	V2, Arveprinsen Ejland	69.76716	51,23323	-	Gyttja	7780±120	8984	8382	164	8591	Isolation contact	Long et al., 1999	46.64	0.38
Beta-112543	V5, Arveprinsen Ejland	69.77402	51.24918	-	Gyttja	6950±150	8159	7509	134	7789	Isolation contact	Long et al., 1999	25.19	0.78
Beta-110748	V7, Arveprinsen Ejland	69.76756	51.25459	-	Gyttja	6290±40	7316	7075	52	7212	Isolation contact	Long et al., 1999	18.01	0.25
Beta-110747	V8, Arveprinsen Ejland	69.76743	51.26005	-	Gyttja	4510±50	5315	4978	94	5159	Isolation contact	Long et al., 1999	13.29	0.93
Beta-110457	V9, Arveprinsen Ejland	69.84323	51.09482	-	Gyttja	3750±130	4516	3725	185	4123	Isolation contact	Long et al., 1999	-2.10	0.37
Beta-110456	V9, Arveprinsen Ejland	69.84323	51.09482	-	Gyttja	1360±90	1467	1061	91	1266	Isolation contact	Long et al., 1999	-2.10	0.37

Table 1: All macrofossil samples in this study are aquatic mosses (bryophytes). All radiocarbon ages were calibrated using OxCal v4.4 (Bronk Ramsey, 2009) and the IntCal20 curve (Reimer et al., 2020), except for sample K-994 which has not been normalised for isotopic fractionation to a delta 13C value of -25 permille i.e., we have added 400 years before calibrating the date into calendar years using Marine20 (Heaton et al., 2020) using a local dR= -49±59 from West Greenland (Pearce et al., 2023). Errors on sill heights in our study are calculated from Coeurdevey & Soubirane (2013).

Core/Lake No.	Latitude °N	Longitude °W	Minimum sill height (m a.s.l.)	Depth at coresite (m)	Lake area (m2)	Length (m)	Width (m)
SAQ21-06	70.026179	51.920846	46.0	5.3	26253	285	140
SAQ21-07	70.020487	51.920420	18.8	4.1	91133	560	290
SAQ21-09	70.042056	52.026509	65.6	9.6	101693	640	270
SAQ21-11	70.044366	52.010009	91.1	5.5	10584	175	80

Table 2: Lake and coring site characteristics.

765